Tetraphenyl Tetrel Molecules and Molecular Crystals: From Structural Properties to Nonlinear Optics

Kevin Eberheim, Christof Dues, Claudio Attaccalite, Marius Müller, Sebastian Schwan, Doreen Mollenhauer, Sangam Chatterjee, Simone Sanna

Tetra-phenyl tetrel molecules and molecular crystals: from structural properties to non-linear optics

Kevin Eberheim,[†] Christof Dues,[†,‡] Claudio Attaccalite,[¶] Marius Müller,[§] Sebastian Schwan,[‖,‡] Doreen Mollenhauer,[‖,‡] Sangam Chatterjee,[§,‡] and Simone Sanna[*,†,‡]

Institute of Theoretical Physics, Justus Liebig University Giessen, Heinrich-Buff-Ring 16, 35392 Giessen, Germany, Center for Materials Research (ZfM), Justus Liebig University Giessen, Heinrich-Buff-Ring 16, 35392 Giessen, Germany, CNRS/Aix-Marseille Université, Centre Interdisciplinaire de Nanoscience de Marseille UMR 7325, Campus de Luminy, 13288 Marseille Cedex 9, France, Institute of Experimental Physics I, Justus Liebig University Giessen, Heinrich-Buff-Ring 17, 35392 Giessen, Germany, and Institute of Physical Chemistry, Justus Liebig University Giessen, Heinrich-Buff-Ring 17, 35392 Giessen, Germany

E-mail: simone.sanna@theo.physik.uni-giessen.de
Phone: +49 (0)641 9933362. Fax: +49 (0)641 9933361

Abstract

The family of group 14 tetra-aryl tetrels with cemical formula $X(C_6H_5)_4$ and X = C, Si, Ge, Sn, Pb is investigated both theoretically and experimentally. Calculations in the framework of the density functional theory are employed to model the structural, vibrational, electronic and optical properties of the clusters, both as single molecules and in their crystalline form. Electronic excitations, optical absorption, second and third harmonic generations are described in detail. Crystalline $X(C_6H_5)_4$ samples with X = Si, Ge, Sn, Pb are grown from solutions by slow evaporation and employed to measure their structural and vibrational properties, as well as their linear and non-linear optical response. The good agreement between calculated and measured properties allows a thorough characterization of the single compounds and yields deep insight in this material class, on the path towards understanding the origin of the characteristic white light emission.

Keywords

tetra-aryl, tetra-phenyl, tetrels, DFT, Raman, SHG, crystals

Introduction

Tetra-aryl tetrels are molecular clusters consisting of a tetravalent central atom binding

[*]To whom correspondence should be addressed
[†]Institute of Theoretical Physics, Justus Liebig University Giessen, Heinrich-Buff-Ring 16, 35392 Giessen, Germany
[‡]Center for Materials Research (ZfM), Justus Liebig University Giessen, Heinrich-Buff-Ring 16, 35392 Giessen, Germany
[¶]CNRS/Aix-Marseille Université, Centre Interdisciplinaire de Nanoscience de Marseille UMR 7325, Campus de Luminy, 13288 Marseille Cedex 9, France
[§]Institute of Experimental Physics I, Justus Liebig University Giessen, Heinrich-Buff-Ring 17, 35392 Giessen, Germany
[‖]Institute of Physical Chemistry, Justus Liebig University Giessen, Heinrich-Buff-Ring 17, 35392 Giessen, Germany

four ligands within the tetragonal symmetry. An intriguing property of the crystalline phase is that the main group element of the periodic system in the central position can be replaced by any other atom in the corresponding group, without changing the essential features of the crystal structure.[1] In particular, tetraphenyl derivatives of silicon, germanium, tin, and lead (all elements of the group 14, see Fig. 1) form thermostable, colorless solids that are not air sensitive and might be either non-toxic (e.g., $GePh_4$), toxic ($SiPh_4$, $SnPh_4$) or extremely toxic ($PbPh_4$).[2] They are popular model systems due to their reduced complexity, which are often used to represent the vast family of compounds with delocalized π-orbitals. Moreover, they are currently employed in optical applications such as organic glasses,[3] light-emitting diodes (LEDs)[4,5] and in the developement of organic LEDs (OLEDs).[6]

All tetraphenyl derivates of the group 14 elements condensate either in an amorphous structure or in a crystalline phase within the space group $P\bar{4}2_1c$ (point group D^4_{2d}). The transparent, highly ordered crystals have often peculiar properties that substantially differ from those of the corresponding powders.[2] Different X-ray diffraction,[7–11] nuclear magnetic resonance (NMR), Raman spectroscopy,[12–16] and infrared spectroscopy (IR) studies[17–20] have been dedicated to these compounds. These studies have proposed efficient synthesis methods,[21] revealed the crystal structures,[22,23] and their optical properties.[24]

Available atomistic models are usually limited to the structural properties of single molecules.[25,26] Lin *et al.*[27] have performed a detailed investigation of the structural and electronic properties of molecular and crystalline $X(C_6H_5)_4$, with X=C, Si, Ge, Sn, Pb within density functional theory (DFT) in the independent particle approximation (IPA). Absorption spectra have been modeled as well. Refined calculations of the linear and non-linear optical response are not available. Indeed, the weak interactions between the molecules, the typical system size, the intra- and intermolecular excitations, as well as the coupling between structural and electronic excitations represent a real challenge for the first-principles modelling of electronic structure and optical response.

Instead, classical models in the framework of the dipole-dipole interaction have been employed to estimate the linear birefringence and optical rotatory power of the crystals, while the dipole-electron shifting model was used to calculate field induced effects including second harmonic generation (SHG), the electro-optic response and electrogyration.[28]

Recently, it has been experimentally shown that tetra-phenyl tetrel crystals show SHG, while the corresponding powders are white light emitters, similar to other tetra-phenyl compounds.[29–33] However, the mechanisms leading to white light generation are far from being understood and lay probably in the intertwinement of electronic and atomic structures and their dynamics.

In order to better understand the interplay between structural and electronic degrees of freedom, we investigate in this work the whole family of group 14 tetra-aryl tetrels, i.e. $X(C_6H_5)_4$ where X = C, Si, Ge, Sn, Pb, both theoretically and experimentally. Structural parameters are calculated, which are in good agreement with measured values and existing literature data. The good agreement of the computed and measured dynamical properties further corroborates the accuracy of the structural models. The electronic structure of single molecules and molecular crystals is calculated at different levels of sophistication and the electronic excitations as calculated by time-dependent DFT (TD-DFT) are discussed in detail. The linear optical properties of the crystals as measured by ellipsometry and optical absorption, and as calculated by DFT are discussed and interpreted in the framework of the intrinsic properties of the molecular constituents. SHG and THG measurements as well as corresponding calculations show a very strong non-linear optical response of all investigated tetra-phenyl derivatives, which is of the same order of magnitude of widely employed non-linear optical crystals such as $LiNbO_3$.

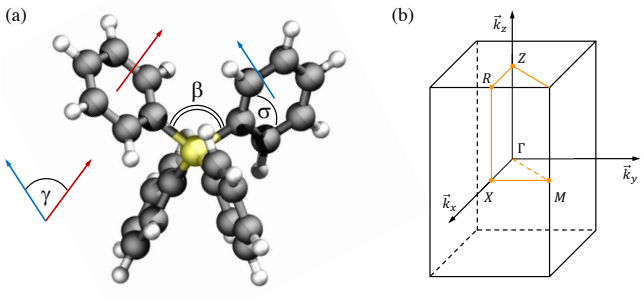

Figure 1: (a) Structural model of the investigated tetra-pheny tetrels. C atoms are gray, H atoms in white and the central atom X = C, Si, Ge, Sn, Pb is yellow. Angles discussed in the following are indicated. (b) Brillouin zone of the tetragonal lattice. The high-symmetry points employed for the calculation of the band structure of the molecular crystals are shown.

Methodology

Computational details

The Vienna ab initio simulation package[34,35] is employed to evaluate the structural, vibrational, electronic and optical properties of the tetra-phenyl tetrels (as isolated molecules or in their crystalline phase) by periodic DFT. Isolated molecules are modeled within a box of 19×20×21 Å. Projected augmented wave pseudopotentials[36,37] are used to describe the ion-electron interaction. The generalized gradient approximation[38] in the PBE formulation[39,40] is used to describe the electronic many-body interactions. The atomic positions are relaxed until the residual Hellmann-Feynman forces[41] are lower than 0.001 eV/Å. The accurate modeling of (in particular, loosely) bonded adsorbate systems is a major challenge for DFT, as (semi)local exchange-correlation (XC) functionals do not properly describe the long-range van der Waals (vdW) interactions. Different *ab initio* as well as semi-empirical corrections schemes are tested. The results presented in this paper are obtained with a semi-empirical DFT-D3 scheme with zero damping,[42,43] which is sufficiently accurate to allow for valid conclusions concerning structural properties. Plane waves up to a cutoff varying between 330 eV ($GePh_4$) and 460 eV ($SiPh_4$) are used as basis for the expansion of electron wave functions. The crystalline phase is modelled within the primitive tetragonal unit cell containing two formula units. A Monkhorst-Pack 2×2×4 k-points mesh[44] for the energy integration of the Brillouin zone ensures numerical convergence.

The cohesive energy of the crystals is calculated as the difference of the total energy of a free standing molecule and a molecule in the crystalline phase as

$$E^{\mathrm{coh}} = (2 * E^{\mathrm{tot}}_{\mathrm{Mol}} - E^{\mathrm{tot}}_{\mathrm{Cryst}})/2, \qquad (1)$$

thus, positive values mark stable crystals.

Phonon modes are calculated within the frozen phonon approach.[45]

While DFT calculations of the electronic ground state considerably underestimate the electronic excitations, reliable values for quasiparticle gaps and exciton energies can be obtained in a very efficient way within the ΔSCF method.[46,47] Within this approximation, quasiparticle gaps are given by the difference

$$E_g^{\mathrm{QP}} = E(N+1,\vec{R}) + E(N-1,\vec{R}) - 2E(N,\vec{R}), \qquad (2)$$

where $\vec{R}$ represents the equilibrium geometry and N the number of electrons in a neutral system. This difference can be interpreted as the difference between ionization energy and electron affinity. As the quantities in Eq. 2 are computed using charged cells, interactions between periodic images affect the calculations. However, the E_g^{QP} depend linearly on $1/L$, where L is the cell side. Thus, using cells of different size and extrapolating to $L \to \infty$, we obtain the corrected values shown in this work.

The lowest excitonic excitation, represented by a hole h in the HOMO and an electron e in the LUMO, is estimated by

$$E_{\mathrm{ex}} = E(e-h,\vec{R}) - E(N,\vec{R}), \qquad (3)$$

whereby $E(e-h,\vec{R})$ is the energy of the system with an electron-hole pair at the ground-state equilibrium geometry $\vec{R}$.

We remark that the ΔSCF approximation holds for isolated molecules and is not valid for the molecular crystals, where more refined

methods such as hybrid-DFT[48] or the GW-approximation[49] are required to account for quasiparticle effects. Hybrid-DFT calculations are performed in this work by modeling the electron exchange and correlation energy with the Heyd-Scuseria-Ernzerhof (HSE06) screened hybrid functional,[50] in which 25% Hartree-Fock exchange is included in the the short-range component of the the PBE-type XC description.

The imaginary part of the frequency dependent dielectric tensor $\varepsilon^i_{\alpha\beta},\ \alpha,\beta = x,y,z$ is calculated following the approach proposed by Gaidoś *et al.*, as sum over empty states at each point of the first Brillouin zone.[51] The real part of the dielectric tensor $\varepsilon^r_{\alpha\beta}$ is not directly calculated, but obtained by Kramers-Kronig relations, and converges, therefore, slowly with the number of empty sates considered in the calculation. We consider thereby 60 filled and 340 empty states for the isolated molecules and 120 filled and 680 empty states for the molecular crystals.

The dielectric function of isolated molecules is obtained averaging the diagonal components ε_{jj} of the dielectric tensor as calculated by DFT-PBE or hybrid-DFT:

$$\varepsilon(\hbar\omega) = \frac{1}{3}\sum_{j=x,y,z}\varepsilon_{jj}(\hbar\omega). \tag{4}$$

The absorption coefficient $\alpha(\omega)$ is calculated as

$$\alpha(\omega) = \sqrt{2}\frac{\omega}{c}\sqrt{\sqrt{(\varepsilon^i_{jj}(\omega))^2 + (\varepsilon^r_{jj}(\omega))^2} - \varepsilon^r_{jj}(\omega)} \tag{5}$$

where c is the light speed in vacuum and $\varepsilon^r(\omega)$, and $\varepsilon^i(\omega)$ are the real and imaginary part of the dielectric tensor, respectively. $jj = xx, yy$ labels the ordinary optical axis, $jj = zz$ the extra-ordinary optical axis. Similarly, the refractive index is calculated as

$$n_j(\omega) = \sqrt{\frac{1}{2}\sqrt{(\varepsilon^i_{jj}(\omega))^2 + (\varepsilon^r_{jj}(\omega))^2} + \varepsilon^r_{jj}(\omega)}, \tag{6}$$

while the birefringence is defined as

$$\Delta n = n_o - n_e. \tag{7}$$

The non-linear optical response is calculated with two distinct approaches. The second order optical susceptibilty $\chi^{(2)}$ is calculated by expressions obtained in perturbation theory,[52] in which two and three band contributions are computed evaluating the momentum matrix elements.[53] Hyperpolarizabilities of in principle any order (in our case $\chi^{(2)}$ and $\chi^{(3)}$) are furthermore calculated in the time-domain by developing the dynamical polarization in a power series of the applied field[54,55]

$$\begin{aligned} P_\alpha = & \sum_\beta \chi^{(1)}_{\alpha\beta}E_\beta + \\ & \sum_{\beta,\gamma} + \chi^{(2)}_{\alpha\beta\gamma}E_\beta E_\gamma + \\ & \sum_{\beta,\gamma,\delta}\chi^{(3)}_{\alpha\beta\gamma\delta}E_\beta E_\gamma E_\delta + \ldots \end{aligned} \tag{8}$$

where $\chi^{(n)}$ is the n-th order frequency dependent susceptibility and E_β is the cartesian component in β direction of the electric field. The dynamical polarization is calculated within the Berry-phase formulation.[56] The frequency-domain and the time-domain approaches yield results in excellent agreement with each other.

Non periodic DFT calculations are carried out using the software package TURBOMOLE v7.3.[57] Structural optimizations are performed with the RIDFT program,[58] the PBE density functional,[39,59,60] and grid size m^3. Single molecules are taken from the crystal structure as initial configurations for the structural optimizations. The calculations are based on point group C_1. The convergence criterion of the iteration cycle is set to 10^{-7} Hartree. Dispersion correction is utilized in Grimme's D3 scheme with Becke-Johnson damping.[42,43,61] The elements H, C, Si and Ge are modeled in an all electron description using the correlation consistent (cc-pVTZ) Dunning-type basis set,[62,63] while for the elements Sn and Pb the energy-consistent scalar-relativistic effective core potential ECP60MWB is employed, in combination with the corresponding basis sets (cc-pVTZ-PP).[64,65] Frequency calculations are performed to confirm the presented stationary

points as minima. In some cases, low imaginary frequencies (in the range of $-1\,\mathrm{cm}^{-1}$ to $-12\,\mathrm{cm}^{-1}$) are found, which can be identified as rotational contributions of the substituents.

Electronic excitations are investigated by means of time-dependent density functional theory (TD-DFT),[66,67] using the ESCF program[68,69] with the exchange-correlation functionals PBE and PBE0,[39,59,60,70] and cc-pVTZ (cc-pVTZ-PP) basis sets. 20 excited states are calculated for the singlet and triplet states. Of these, the four lowest singlet states and the three lowest triplet states, whose oscillator strength are non-zero, are used for analysis. The triplet and singlet excitations are calculated in spin-unrestricted calculations. The spin contamination deviation is always less than 3%, except for the calculations of the triplet excitations using the PBE0 functional. These calculations show strong spin contamination (>10%) and are therefore not used for the analysis. However, the results are given in the SI.

Crystal growth

[XPh_4] single crystals with X = Si, Ge, Sn, Pb are grown by slow evaporation from saturated solution of chloroform at room temperature. The compound forms long needles along the c-axis[71] with square cross-section of about 1 cm length and high crystalline quality, as shown in Fig. 2. The crystals belong to the tetragonal space group $P\bar{4}2_1c$, with the lattice parameters reported in Tab. 2. These are in very good agreement with previous experiments[22] and with the DFT calculations shown in the following.

Experimental setup

Raman measurements are performed on a commercially available confocal Raman microscope (Renishaw inVia Qontor) using a HeNe Laser at 632.8 nm for excitation. We use a PerkinElmer Lambda 900 spectrometer for the linear absorption measurements covering the spectral range from 220 nm to 800 nm. The linear absorption is derived from transmission data on single crystals and from solution in chloroform with a concentration of 2 mmol/l. We use a 50 fs pulse duration 5 kHz repetition rate Ti:Sa amplifier to drive a optical parametric amplifier including mixing stages to generate sub-100 fs pulses from 700 nm to 1620 nm. SHG is measured by placing the crystal in the focused beam ($f = 10$ cm) under normal incidence. For detection, a Si-photodiode and a lock-in amplifier are used. The fundamental laser is suppressed by appropriate dielectric short-pass filters. The data is corrected against a simultaneously acquired reference on z-cut quartz for which the absolute value of $d_{11} = 0.3\,\mathrm{pm/V}$ at 1064 nm is known.[72] We use Miller's constant-delta condition[73] with a Miller delta of $\delta_{11} = 1.328 \cdot 10^2\,\mathrm{m/C}$ to account for the dispersion of the second-order nonlinear coefficient of the quartz reference, as already performed, e.g., in Ref.[74] The complete spectral response is measured using the same laser for excitation, as well as a Czerny-Turner monochromator and a back-illuminated Silicon-CCD-camera for detection.

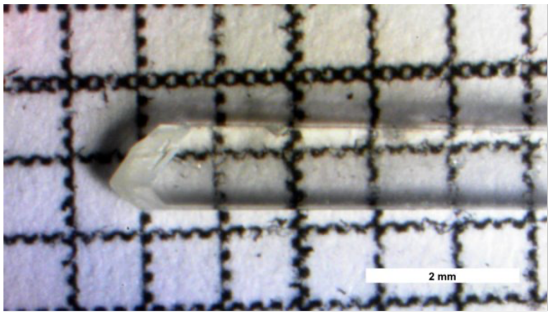

Figure 2: The XPh_4 compounds forms long needles along the c-axis with square cross-section of about 1 cm length and high crystalline quality. The as grown [$SiPh_4$] crystal is exemplarily shown.

Ellipsometric measurements are performed with an SEN research 4.0 spectroscopic ellipsometer in the range from 190 nm to 1040 nm. The sample crystal is rotated around an ordinary axis and multiple measurements are taken at different rotation and incidence angles. The whole dataset is simulated using Berreman's 4×4 matrix method[75] implemented as an python package[76] in the transparent region. The dielectric function of the crystals are described with a Sellmeier model.

Single crystal XRD spectra are recorded at

100 K in an Bruker D8 VENTURE diffractometer with a Mo-K_α source.

Results and discussion

Structural properties

Isolated molecules

After structural relaxation, all molecules of the investigated tetra-phenyl compounds display the tetrahedral symmetry S_4, determined by the sp^3 hybridization of the central tetrel atom, and are very similar to each other. According to the S_4 symmetry, the six angles β between two phenyl rings shown in Fig. 1 splits into two groups (β_1 and β_2) containing angles which are larger and smaller, respectively, than the ideal angle of 109.5° characteristic for the sp^3 hybridization. The average of the calculated values is reported in Tab. 1 and is in very good agreement with previous calculations.[27] While C, Si, Ge, and Sn compounds have four β_1 and two β_2 angles, Pb has two β_1 and four β_2 angles. The average of β_1 and β_2 is for all compounds very close to to the perfect tethraedral angle of 109.5° of the T_d symmetry. The largest deviation from this symmetry is calculated for the CPh_4 compound.

The geometry of the phenyl rings does not significantly change upon attachment to the tetrel atom. However, the calculated angles σ between 117.79° and 119.59° show that the phenyl rings are slightly elongated, as firstly pointed out by electron diffraction measurements of the gas phase.[77] The calculated σ values are in very close agreement with the measured values reported in the liteature.[77] Also in this case, CPh_4 shows the largest distortion.

The X-C bond length grows with the atomic number of the X atom and closely matches the sum of the covalent radii of carbon and the X species. This suggests a mainly covalent nature of this bond. The calculated values closely match corresponding measurements.[77] The relative orientation of the phenyl rings is almost identical for all considered tetrels. The angle γ that quantifies this quantity is between 66° and 67°. Calculations with larger cells do not lead to appreciable structural modifications.

Table 1: Averaged structural properties of tetra-phenyl tetrels single molecules as calculated within DFT. R_X^C is the single bond covalent radius of atom X = C, Si, Ge, Sn, Pb. Angles β, σ and γ are defined in Fig. 1.

	CPh_4	$SiPh_4$	$GePh_4$	$SnPh_4$	$PbPh_4$
R_X^C [Å]	0.75	1.16	1.21	1.40	1.44
X−C [Å]	1.551	1.883	1.976	2.265	2.263
β_1 [°]	111.50	110.02	110.07	110.20	110.35
β_2 [°]	105.50	108.38	107.92	107.98	107.72
σ [°]	117.79	117.96	118.78	118.74	119.59
γ [°]	66.58	66.02	66.06	66.70	66.73

Molecular crystals

Symmetric tetra-aryl molecules usually crystallize in tetragonal space groups, with the molecules located on sites of 4 symmetry (i.e., again S_4). Within tetragonal crystals, the molecules are stacked in columns with (roughly) squared cross sections, which grow parallel to the z axis (also called c axis). Thereby, the aryl-groups of neighboring columns are interleaved in herringbone-like structures. Due to this arrangement, tetra-aryl molecules often retain their symmetry in the crystals. Tetraphenyl tetrels are no exception, as the XPh_4 units fit together to form columnar stacks (see Fig. 3) in which the phenyl groups occupy the empty $\overline{4}$ sites.

The structural details of the optimized crystal structures are compiled in Tab. 2, together with available literature data for comparison. The C-C distance within the phenyl rings of the considered tetraphenyls does not substantially differ. Following the notation of Ref.,[22] we define the valence angle α as the angle between the XC_1C_4 direction and the c axis, so that $\alpha = \sphericalangle\, C_1(I)XC_1(III)/2$. Two parameters describe the relative orientation of the XPh_4 molecules within the unit cell. ω describes the rotation of the phenyl ring about the XC_1 direction, and is defined as the angle between the ring plane and the $C_1(I)XC_1(III)$ plane. φ is the angle between the b axis and the projection of the XC_1 direction on the ab plane. This defines the rotation

of the whole molecule about the c axis.

Table 2: DFT calculated and measured lattice parameters of crystalline tetraphenyl tetrels.

	a [Å]	c [Å]	c/a	α	ω	φ	E^{coh}
C	10.84[a]	7.12	0.657	53.4	48.62	6.92	1.65
	10.87[b]	7.23	0.665			7.5	
	10.92[c]	7.29	0.668				
	10.91[d]	7.29	0.668	53.4			
	11.04[e]	7.42	0.672	53.4	48.6		0.55
Si	11.44[a]	6.78	0.593	54.1	51.84	7.00	1.71
	11.30[b]	7.05	0.624			8	
	11.45[c]	7.06	0.617				
	11.44[d]	7.06	0.617	54.0			
	11.56[e]	7.20	0.622	54.6	52.3		0.79
	11.48[f]	6.76	0.589				
Ge	11.00[a]	6.53	0.577	54.2	56.89	7.90	0.92
	11.60[b]	6.85	0.591			7	
	11.66[c]	6.92	0.593				
	11.62[d]	6.90	0.594	54.2			
	11.75[e]	7.02	0.598	54.0	53.6		0.65
	11.70[f]	6.53	0.558				
Sn	11.34[a]	6.52	0.575	54.0	57.44	7.99	1.35
	11.85[b]	6.65	0.561			7	
	12.06[c]	6.58	0.546				
	12.07[d]	6.56	0.543	55.5			
	12.22[e]	6.69	0.547	55.2	58.1		0.70
Pb	11.50[a]	6.75	0.587	53.6	56.95	8.08	1.65
	12.09[b]	6.59	0.546	55.8	58.9	7.5	
	12.14[c]	6.55	0.540				
	12.11[d]	6.54	0.540	55.6			
	12.25[e]	6.67	0.545	55.1	58.1		0.77
	12.05[f]	6.40	0.531				
	12.03[g]	6.55	0.545			5.5	

[a]This work ; [b]Exp.[22] ; [c]Exp.[28] ; [d]Exp.[1] ; [e]Theo.[27] ; [f]Exp. this work ; [g]Exp.[78] ;

Table 2 shows that the calculated structural parameters are in overall satisfactorily agreement with measured and previously calculated data. However, the scattering of the measured values points out the difficulty in growing highly ordered crystals, which, in turn, suggests that real samples might contain a large quantity of structural defects. Thus, caution is due when comparing the experimental results with the theoretical predictions.

As a general trend, the lattice parameter a grows and the lattice parameter c decreases, respectively, with growing atomic number. Thereby, CPh_4 show the highest c/a ratio, i.e., the lowest anisotropy. This is also visible in the optical response, as we shall see in the following.

As expected, our calculations show that the overall molecular form is retained upon crystallization, and also the predicted distortion is minor. The $X-C_1$ bond length does not substantially change (from 0.0 % in CPh_4 to 0.8 % in $GePh_4$). The relative orientation of the phenyl rings, quantified by the angle γ between the phenyl planes, is modified upon crystallization. While the angle γ is substantially the same for all the phenyl rings in the isolated molecules, it depends on the considered rings in the condensed phase, due to the crystal anisotropy. However, the relative orientation of different rings remains between 62.5° and 68.1° and thus within 5% of the value predicted for the single molecules. The angle φ grows with the period of the central atom, instead.

Cohesive energies of about 1 eV per molecule suggest the formation of relatively stable crystals. Our models systematically overestimate the cohesive energy previously calculated within DFT and a localized basis.[27]

The optimized atomic structures of isolated molecules and molecular crystals are the basis for the following calculations of vibrational, electronic and optical properties.

Vibrational properties

As discussed in the introduction, the vibrational properties of tera-phenyl derivates have been explored by Raman and infrared spectroscopy in the past. A tentative assignment of the measured spectral features to atomic displacements has been proposed on the basis of classic force constant calculations.[79]

In this work, we calculate the phonon mode frequencies at the Γ-point for all investigated crystals within DFT-PBE and measure the Raman spectrum of XPh_4, X = Si, Ge, Pb. Figure 4 shows the comparison between calculated (blue bars) and measured (red line) data exemplarily for $SiPh_4$, while Fig. 5 represents a comparison of the frequencies calculated for the different crystals and Fig. 6 of the measured spectra.

The comparison between measured and calculated data demonstrates a very good agreement

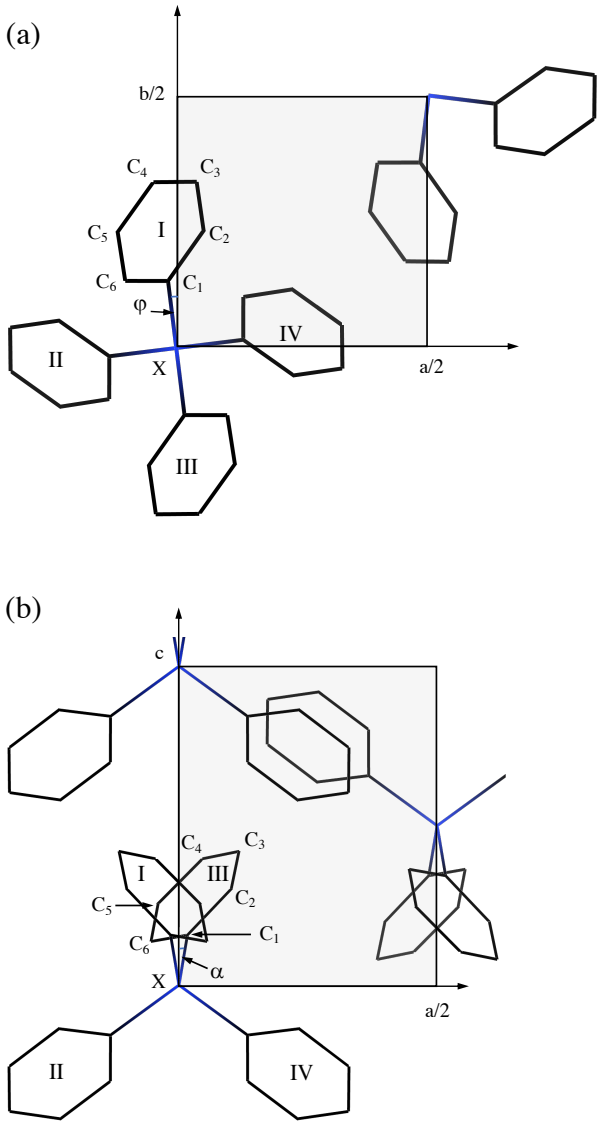

Figure 3: Schematic representation of the projections of the [Si(Ph)$_4$] crystal (a) on the *ab* and (b) on the *ac* plane.

between experiment and theory. The largest deviation between measured and calculated frequencies occurs for the modes above 3000 cm^{-1}, and is below 3%.

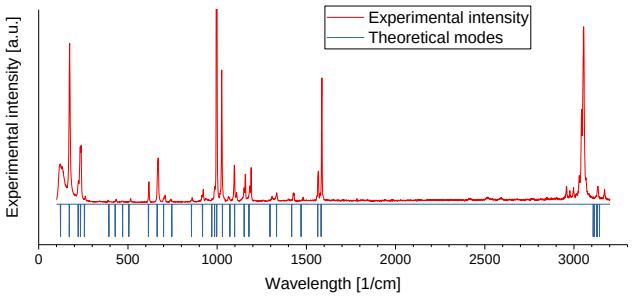

Figure 4: Comparison of the measured phonon spectrum of crystalline SiPh$_4$ with the phonon frequencies calculated within DFT.

The calculations allow us to assign displacement patterns to the measured spectral features. We observe (see e.g., PbPh$_4$ in Fig. 5) that the phonon modes tend to cluster into groups of similar frequency. All modes above 3000 cm^{-1} are modifications of the C-H bond in the phenyl rings. These modes have nearly identical frequencies for all investigated compounds.

Modes with wavenumber about 1500 cm^{-1} and down to 600 cm^{-1} are distortions of the phenyl rings, due to the displacement of the C atoms within the phenyl plane. Also for these modes the same groups are observed for all investigated tetrels. However, as the symmetry of the phenyl rings increases with the period of the central atom (see, e.g., value of the angle σ in Tab. 1) the mode degeneracy also increases within the group 14 from C to Pb. For this reason, the spectrum of PbPh$_4$ looks more compact in this region than CPh$_4$ or SiPh$_4$. The smaller vibration amplitude of the heavier elements such as Sn ang Pb is also expected to induce a lesser structural distortion and thus lead to a more compact spectrum.

Below 500 cm^{-1}, distortions of the phenyl rings out of the phenyl plane or affecting the X-C bond length occur. Obviously, the differences of the X-C bonds for X=C, Si, Ge, Sn, Pb and the different mass of the central atom play a major role in this region, and the phonon

frequency of the corresponding modes for the investigated crystals is somewhat different.

The phonon modes of lowest wavenumber are breathing modes, rigid translations of the phenyl rings with respect to the central atom, and rotations of the phenyl rings. These are of very similar energy for all compounds.

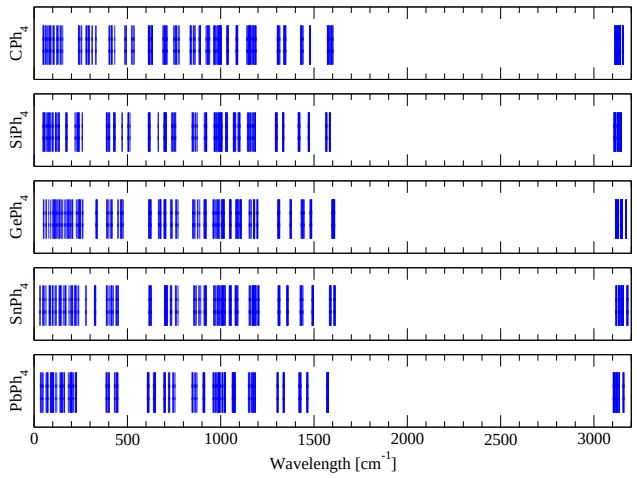

Figure 5: Comparison of the phonon frequencies at the Γ point calculated within DFT-PBE for the crystalline XPh_4 derivates with X=C, Si, Ge, Sn, and Pb.

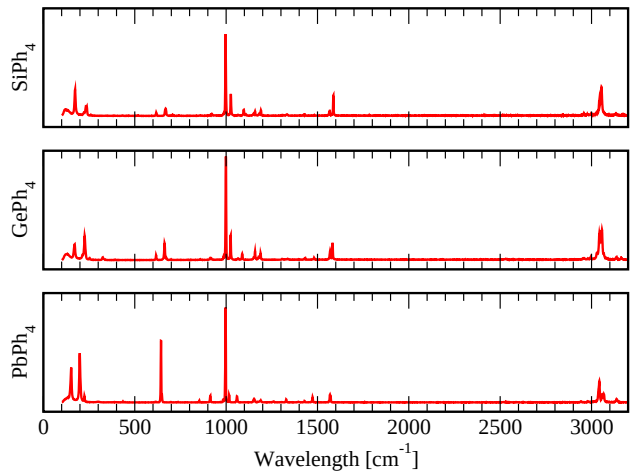

Figure 6: Comparison of the Γ point Raman shifts measured for the crystalline XPh_4 derivates with X = Si, Ge, and Pb.

Table 3: Electronic structure properties of tetra-phenyl tetrel single molecules as calculated within DFT and in the ΔSCF approximation.

	CPh_4	$SiPh_4$	$GePh_4$	$SnPh_4$	$PbPh_4$
E_g^{PBE}	4.18	4.40	4.51	4.57	4.55
E_g^{HSE06}	5.22	5.47	5.59	5.68	5.68
E_g^{QP}	6.91	7.00	7.01	6.97	7.22
E_{ex}	4.01	4.01	4.34	4.43	4.39

Electronic properties

Isolated molecules

Tab. 3 shows the data related to the electronic structure of the isolated tetra-phenyl molecules. As a general rule of thumb, the HOMO-LUMO energy difference grows with the atomic number from C to Pb. The exact order depends on the computational approach, however, the HOMO-LUMO gaps are of very similar magnitude. The values calculated within DFT-PBE are expected to underestimate the energy gap (4.2 eV-4.6 eV, see also Fig. 7, blue lines), while the quasiparticle energies E_g^{QP} yield more realistic values (6.9 eV-7.2 eV). Hybrid-DFT calculated values are between DFT-PBE and quasiparticle gaps (Fig. 7, red lines).

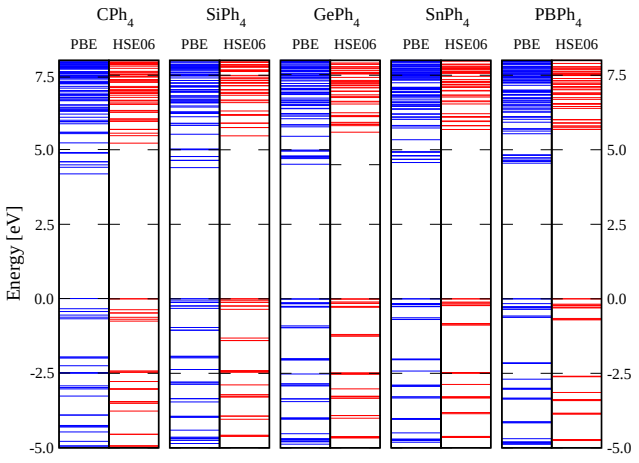

Figure 7: Comparison of the molecular orbital energies calculated for the single molecules of the investigated tetra-pheny tetrels within DFT-PBE and by hybrid-DFT. The HOMO level is the energy zero.

HOMO and LUMO orbitals as calculated within DFT-PBE are shown in Fig. 8. The

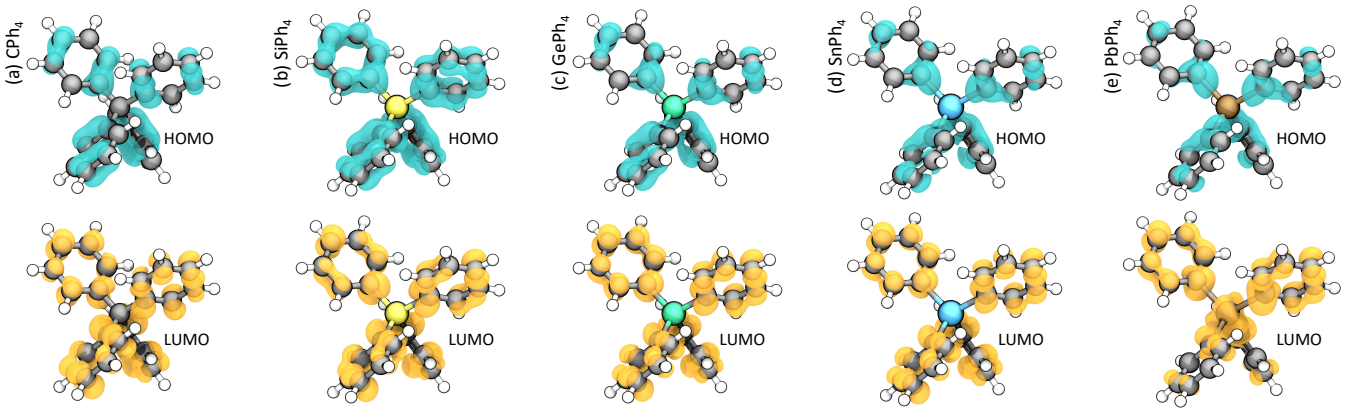

Figure 8: Comparison of the DFT calculated HOMO and LUMO for the single molecules of the investigated tetra-pheny tetrels. The orbital character does not substantially differ for the considered tetra-phenyl derivates.

orbital character does not substantially differ for the considered tetra-phenyl derivates. The HOMO orbitals are reminiscent of the rather delocalised π-orbitals at the phenyl rings, as clearly visible, e.g., for $SiPh_4$. With increasing atomic number, the HOMO orbitals shift toward the central atom. The LUMO orbitals resemble p-orbitals, instead. Also for the LUMO orbitals, the contribution of the central atom grows from CPh_4 to $PbPh_4$. We observe that HOMO and LUMO have a strong spatial overlap, which facilitiates HOMO-LUMO electronic transitions. The orbital form as well as the HOMO-LUMO energy gaps are consistent with data previously calculated with a local basis set.[27]

Tab. 3 shows that the lowest electron-hole excitation E_{ex} has a very similar energy to the DFT HOMO-LUMO gap for all investigated tetrels. This suggests that quasiparticle effects and electron-hole attraction have roughly the same magnitude, and that optical excitation spectra (such as the absorption spectra shown in the following) calculated within the independent-particle approximation might be in good agreement with the experimental data due to a large error cancelation.

Molecular crystals

When the single tetra-phenyl molecules crystallize into ordered, periodic structures, the discrete molecular energy levels become broader energy bands as shown in Fig. 9. For all investigated compounds, the electronic band gap of the molecular crystal is somewhat smaller than the difference of the HOMO and LUMO energies of the parent molecules.

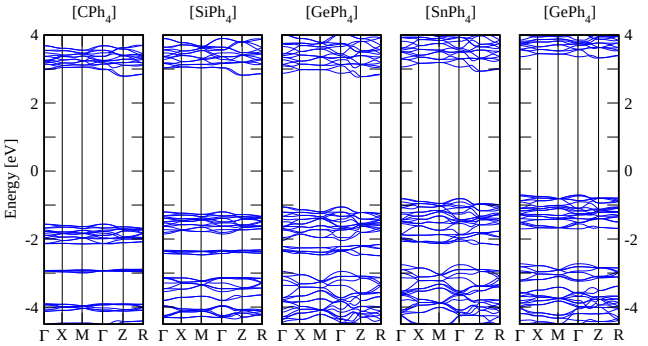

Figure 9: Comparison of the DFT calculated band structures of the molecular crystals of the investigated tetra-pheny tetrels. The high-symmetry points of the Brillouin zone are shown in Fig. 1.

All the band structures show a very limited dispersion, which is typical for molecular crystals. Besides the fundamental band gap energy (3.5 eV to 4.5 eV), several sub-gaps appear in the valence band, which play a role in the linear and non-linear optical response. The absolute squared wave functions of the states associated with the valence band maxiumum and conduction band minimum are shown representatively for $[(PhSi)_4]$ crystals in Fig. 10.

We note that the orbital character of the valence band and conduction band edges of the

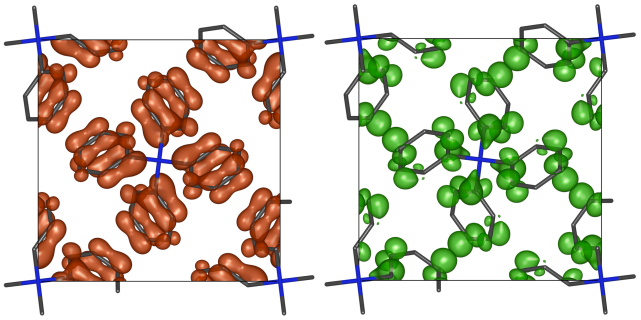

Figure 10: Absolute squared wave functions associated to the highest occupied band (lhs) and to the lowest unoccupied band of [$(PhSi)_4$] crystals as calculated with DFT-PBE. The projection on the ab plane is shown. Other [$(PhX)_4$] tetrels do not substantially differ.

crystals strongly resemble those of the HOMO and LUMO of the parent tetra-phenyl tetrel molecules (see Fig. 8). The valence band maximum has the typical form of the π-orbitals and is localized at the phenyl rings, while the conduction band minimum strongly resembles the carbon p-orbitals.

Optical properties

Tetraphenyl crystals are transparent in a rather wide range covering the visible and near infrared region (325 nm to 1200 nm)[71] and are thus intersting for a multitude of optical applications. Atomistic calculations allow to determine to which extent the optical response of the molecular crystals is dominated by the intrinsic properties of the molecular constituents or rather results from their interaction in the solid state. We therefore discuss first the properties of the single molecules and compare it with the molecular crystals.

Linear optics

Figure 11 shows the dielecric function (imaginary part, $\varepsilon_i(\hbar\omega)$) as calculated for the tetraphenyl derivates from the eigenvalues and eigenfunctions in the DFT-PBE independend particle approximation (blue line) or by hybrid-DFT (red line). The form of the dielectric function is roughly the same for all investigated compounds, although the spectral features appear blue shifted with increasing atomic number. This is not surprising, as the transitions determining the optical answer are the same for all compounds, even if they occur at slightly different energies.

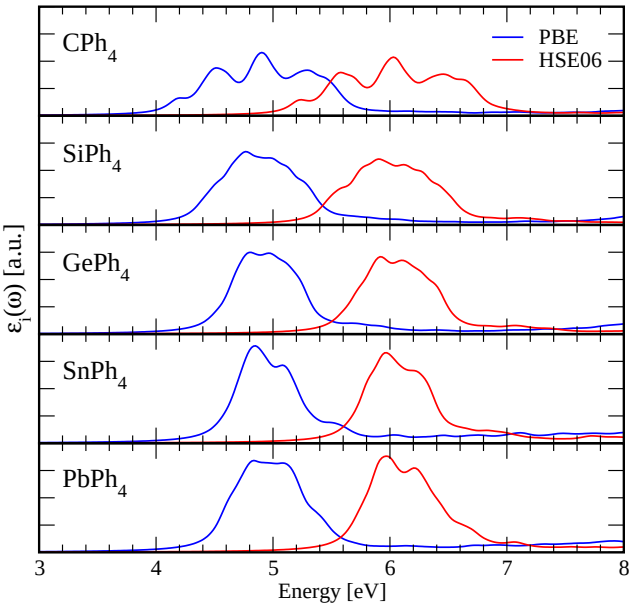

Figure 11: Comparison of the imaginary part of the averaged dielectric function of the investigated tetra-pheny tetrels (single molecules) as calculated within DFT-PBE and hybrid DFT.

The first adsorption peak roughly matches the HOMO-LUMO energy difference. Due to the localization of both states at the phenyl rings, the corresponding transition probability is rather high. Transitions involving higher empty states lead to the further peaks.

As the geometry of the tetra-phenyl molecules is not strongly modified upon crystallization, no drastic differences in the dielectric function of the single molecules and of the crystals are expected. The calculated dielectric function of the tetra-phenyl crystals is shown in Fig. 12. It strongly resembles in each case the corresponding curve in Fig. 11, although spectral features are less sharp, as the energy levels of the single molecules become broader energy bands in the crystals. Furthermore, appreciable differences are computed for the ordinary and extraordinary optical axis, which become more pronounced in the resonant region from C to Pb, mirroring the differences in the c/a ratio

of the lattice parameters. The calculated ordinary and extraordinary refractive index as well as the birefringence are reported in Tab. 4 for a typical laser wavelength λ=650 nm (1.91 eV) in the (non-resonant) visible range. The calculated birefringence nicely reproduces available experimental values[28] are alsr reported in the table (in parenthesis) for comparison.

Table 4: Ordinary (n_o) and extraordinary (n_e) refractive index and birefringence calculated within hybrid DFT for the [XPh_2] crystals at a typical laser wavelength λ=650 nm (1.91 eV). Experimental values from Ref.[28] are reported (in parenthesis) for comparison.

	CPh_4	$SiPh_4$	$GePh_4$	$SnPh_4$	$PbPh_4$
n_o	1.831	1.798	1.943	1.894	1.874
n_e	1.807	1.757	1.860	1.824	1.818
Δn	0.024	0.041	0.082	0.070	0.055
	(0.030)	(0.036)	(0.045)	(0.083)	(0.050)

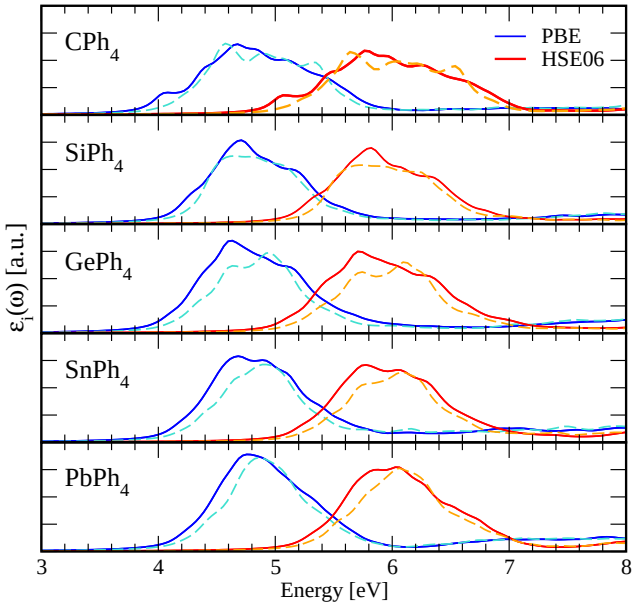

Figure 12: Comparison of the imaginary part of the dielectric function of the investigated tetrapheny tetrels (crystalline phase) as calculated within DFT-PBE and hybrid DFT. Solid and dashed lines represent the ordinary and extraordinary optical direction, respectively.

Besides the optical anisotropy, no features are predicted in the calculations, which might suggest the formation of new covalent bonds upon crystallization, so that the optical response of the molecular constituents largely determines the optical response of the molecular crystals.

The calculated dielectric functions are in good agreement with the measured spectra. This is shown in Fig. 13, in which the real part of the dielectric function as measured by ellipsometry (exemplarly for $PhSi_4$) and as calculated by hybrid-DFT are compared. The measured values (a fit to the Sellmeier equations applicable in the transparency region is shown) as well as the calculated values are furthermore in agreement with literature values.[28]

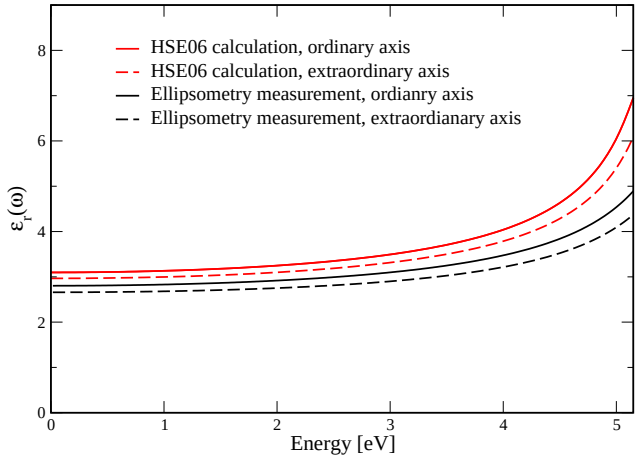

Figure 13: Comparison of measured and calculated dielectric function of [$Si(Ph)_4$] crystals. See text for details.

On the basis of the dielectric function shown in Fig. 12, linear optical spectra can be calculated. Figure 14 shows the absorption spectra measured and calculated for XPh_4 in $CHCl_3$ solution (lhs), and for [XPh_4] crystals (rhs). The spectral feature measured for the heavier [XPh_4] crystals at about 3.8 eV is related to singlet-triplet transitions,[80] which are discussed later in the manuscript for the single molecules. The calculated optical absorption edge is compatible with the measured curves, although the calculated spectra appear slightly red shifted. This could be due both to the solvent (not considered in the calculations) concerning the isolated molecules, or a consequence of the typical underestimation of the fundamental bandgap within DFT. Yet, the satisfactory agreement between theory and experiment further corroborates the quality of the computa-

tional approach and confirms that, due to a favorable error cancelation, the calculations at the IPA level might correctly describe the optical response of the investigated system. Indeed, the experimentally measured optical bandgap of about 4.4 eV is in good agreement with the value calculated by DFT-PBE (see Tab. 3).

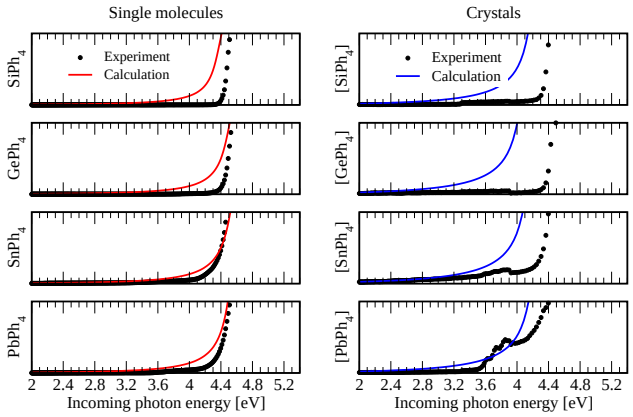

Figure 14: Comparison of measured and calculated optical absorption of XPh_4 single molecules and $[X(Ph)_4]$ crystals, for X = Si, Ge, Sn, and Pb. The experiments are performed for $X(Ph)_4$ molecules in $CHCl_3$ solution. Optical absorption in arbitrary units.

Additional insight into the optical properties of the materials can be achieved by calculating the low lying singlet and triplet excited states of the isolated molecules, see Fig. 15. The low-lying excitations for the various chemical systems are all $\pi_{CC}\pi^*_{CC}$ excitations in which similar orbitals are involved. These are presented in the SI. For the singlet excitations, the overall trend for the different structures for the low-lying excitations calculated with PBE and PBE0 agrees qualitatively. However, the excitation energies calculated with PBE are underestimated by 1.2 eV to 1.5 eV with respect to PBE0. For the calculated triplet excitations there is a strong spin contamination obtained with the PBE0 functional, so that only the PBE results are used for the evaluation.

Figure 15 shows that the energy for the first singlet excitation from S_0 to S_1 increases with increasing molecular weight (C<Si<Ge<Sn<Pb). The second excitation from S_0 to S_2 also increases from central atom C to Sn, but decreases again from Sn to Pb. The third and fourth singlet excitations show a nearly constant variation from C to Pb with a small deviation from C to Si (PBE0). For the spin-forbidden triplet excitations, the excitation energies increase from C to Pb for the three lowest excitations, and decrease from Sn to Pb for the third excitation. The overall excitation energies are slightly lower than those of the corresponding singlet excitations.

Non-linear optics

As crystals belonging to the $P\bar{4}2_1c$ space group lack inversion symmetry, non-linear optical properties might be expected.[1] Indeed, tetraphenyl tetrels have been found to be SHG sources and proposed as design elements in crystal engineering.[6,28]

Crystal of the tetragonal symmetry $\bar{4} = S_4$ have at most six distinct and non-vanishing components of the $\chi^{(2)}$ tensor:[81,82]

$$\begin{aligned} xyz = yxz, \quad xzy = yzx, \quad xzx = yzy, \\ xxz = yyz, \quad zxx = zyy, \quad zxy = zyx. \end{aligned} \tag{9}$$

We have explicitly calculated all the 27 tensor components both within the frequency-domain and within the time-domain with the approaches described before. The two approaches are in excellent agreement and show no qualitative difference. Therefore we only show the results computed with the momentum matrix approach. As expected, most components are exactly zero due to the crystal's symmetry, such as the xxx, yyy or the zzz component. Other components are nonzero but vanishing small (i.e., < 0.001 pm/V), such as the $zxx = zyy$ component. Six components are finite and of noticeable magnitude: $zyx = zxy$ and $xyz = yxz = xzy = yzx$. The non-equivalent zyx and xyz components are shown in Fig. 16 for all investigated tetra-phenyl crystals as a function of the incoming photon energy. They represent electric fields of the incoming light in y and x, as well as in y and z direction, and outgoing photons of doubled frequency ploarized in z and x direction, respectively.

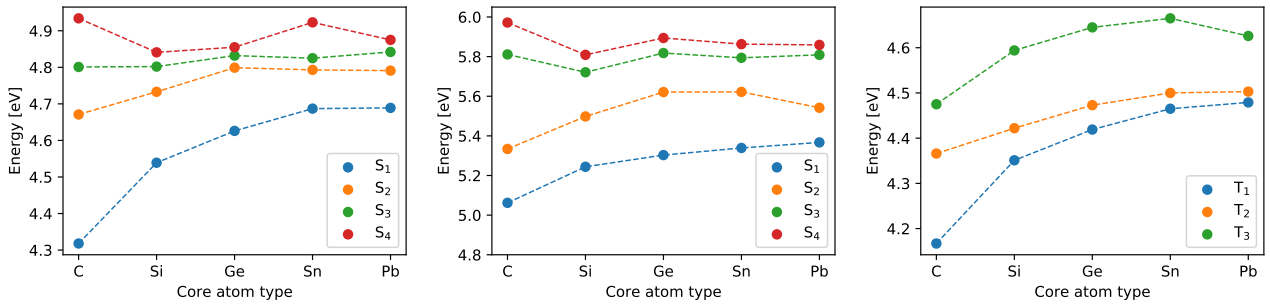

Figure 15: Excitations of the single molecules for the different chemical compositions CPh_4, $SiPh_4$, $GePh_4$, $SnPh_4$, and $PbPh_4$. Left: the first four singlet excitations calculated on PBE-D3(BJ)/cc-pVTZ level of theory, middle: the first four singlet excitations calculated on PBE0-D3(BJ)/cc-pVTZ level of theory, right: the first three triplet excitations calculated on PBE-D3(BJ)/cc-pVTZ level of theory. The corresponding vertical absorption spectra are given in the SI. S represents the singlet states and T the triplet states. The designation S_1, S_2, S_3, etc., shows that the excitation takes place from S_0 to S_1, S_2, S_3, etc.

The zyx tensor component (red curve) of all compounds shows a first peak between 2.0 eV and 2.5 eV. The height of this peak generally grows within the group 14 of the periodic table, from a value of about 15 pm/V for CPh_4 to about 45 pm/V for $PbPh_4$. This value has the same order of magnitude of typical ferroelectric crystals, and thus demonstrates the strong non-linear optical response of tetra-phenyl tetrels. In order to understand the origin of the first peak of the spectrum, we plot the imaginary part of the dielectric function $\varepsilon_i(\hbar\omega)$ (light green curve) as well as the imaginary part of dielectric function as a function of half photon energy (green curve). The first SHG peak occurs exactly at the position of the first maximum of $\varepsilon_i(\hbar\omega/2)$, suggesting a high efficieny of the process doubling the frequency of two photon with half bandgap energy. The maximum of the SHG signal of the zyx tensor component (red curve) corresponds for all investigated compounds roughly to the fundamental gap energy, and is thus located between 4 eV and 5 eV.

The xyz component of the $\chi^{(2)}$ tensor (blue curve) shows optical non-linearities of the same order of magnitude of the zyx component and a similarly diversified spectrum with several minima and maxima. We observe that for both components the minima of the SHG spectrum might come close to 0 pm/V, thus the SHG efficiency is strongly dependent on the frequency of the incoming photons.

Concerning the third-order optical susceptibilities, we find a similar magnitude and form for the diagonal components of the $\chi^{(3)}$ tensor. Therefore, we limit our discussion to the $xxxx$ and $zzzz$ components. Figure 17 shows exemplarily the calculated THG spectrum of the $SiPh_4$ compound, which is dominated by the peak at about 1.5 eV. This peak is as high as about $1.5{\cdot}10^4$ pm^2/V^2 and is, thus, very similar to the THG calculated for optically non-linear crystals such as $LiNbO_3$. As shown in Fig. 17, this peak is located at one third of the fundamental band gap of $SiPh_4$ and fits to the imaginary part of the dielectric function for one third photon energy. It is thus expected to be responsible for the high efficiency of three photon resonances. The THG spectrum shows additional features at higher energies. Though, they are an order of magnitude smaller than the main peak and are not further discussed.

Corresponding experimental data are shown in Fig. 18. The upper panel shows exemplarily for the $SiPh_4$ the good agreement of calculated and measured SHG spectra for incoming photon energies between about 0.75 eV and about 1.15 eV. The theoretically predicted THG resonance at about 1.5 eV is clearly visible in the experimental data, which are shown in the lower panel of Fig. 18 (please, notice the logarithmic

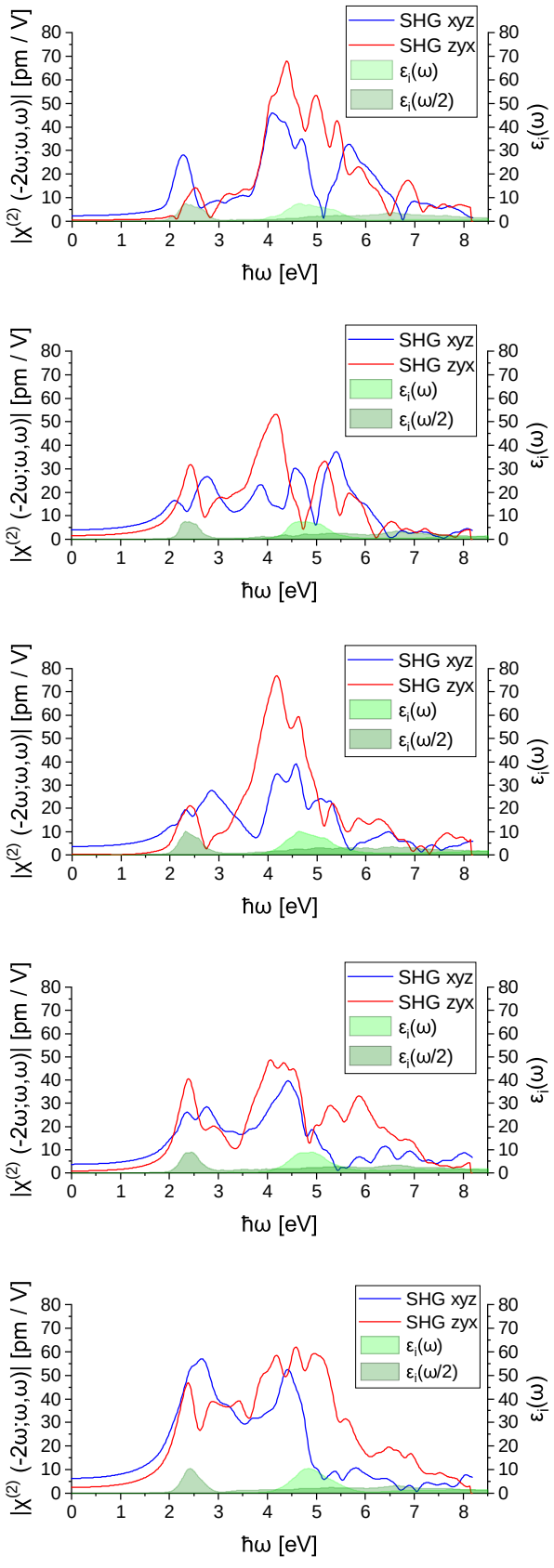

Figure 16: Coefficients of the second-order polarizability tensor $\chi^{(2)}(\omega)$ calculated in the IPA with the momentum matrix approach for the investigated tetraphenyl tetrels.

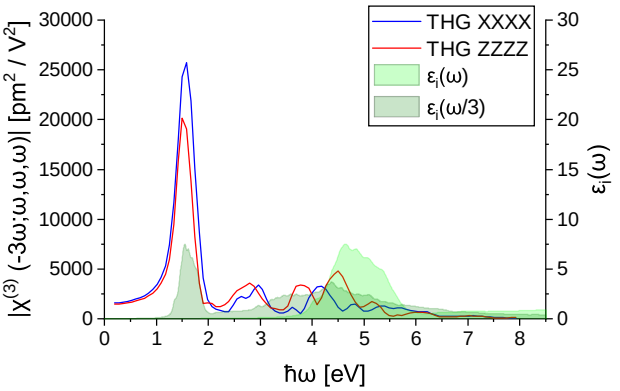

Figure 17: $xxxx$ and $zzzz$ components of the $\chi^{(3)}$ tensor as calculated for the $[Si(Ph)_4]$ crystal within the independent particle approximation in the time-domain approach (blue line). The imaginary part of the dielectric function ($\varepsilon_i(\omega)$ green curve) is shown for comparison as well.

scale). In this picture, the energy resolved intensity of the detected light is displayed. The first peak is related to the THG emission, while the second peak is SHG.

Conclusions

The structural, dynamical, electronic and optical properties of thetra-phenyl derivatives of the group 14 elements C, Si, Ge, Sn and Pb are investigated theoretically and experimentally. Calculations within the periodic supercell method and (semi)local as well as hybrid XC potentials are employed to determine the atomic and electronic structure of single molecules and molecular crystals. Similar HOMO-LUMO gaps and orbital forms are predicted for the different tetra-phenyl tetrels, although the orbital contribution of the central atom grows from CPh_4 to $PbPh_4$. Electronic gaps above 6 eV and optical gaps of about 4.5 eV are predicted for the single molecules. The results are in agreement with existing measurements and previous calculations, and suggest an almost complete compensation of electronic self energy and exciton binding energy for the lowest optical excitation.

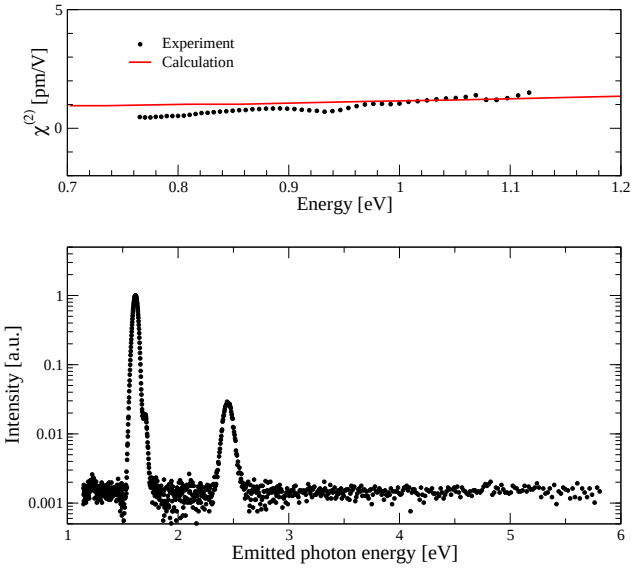

Figure 18: Measured second and third harmonic generation of $[Si(Ph)_4]$ crystals. In the upper panel the SHG intensity is shown as a function of the incoming photon energy. Calculated data shown in Fig. 16 (b) is reported in the upper panel for comparison. The lower panel displays the energy resolved intensity of the detected light by an excitation at 0.83 eV. The first peak is related to the THG emission, while the second peak is SHG.

The linear and non-linear optical response of the crystals are modelled wihin the frequency domain and within the time domain, and measured in specifically grown $[XPh_4]$ crystals. According to our calculations, the optical response of the crystals is largely dominated by the parent molecules. No new covalent bonds are created upon crystallization, which qualitatively modify the spectral features of the single molecules. The models correctly reproduce the measurements and predict a strong non-linear optical response for all investigated molecular crystals, which is of comparable magnitude of largely employed non-linear optical crystals such as $LiNbO_3$.

As the optical properties of the tetra-phenyl tetrels strongly resemble those of more complex tetra-phenyl molecules such as $[(PhSi)_4S_6]$, it can be assumed that the central part of the cluster has only a moderate role in the optical response. This also holds for white light generation processes. For this reason, tetra-phenyl tetrels are a good model system, which can be employed to understand processes exploited in more complex molecular clusters.

Acknowledgement We express our gratitude for funding by the German Research Foundation (Deutsche Forschungsgemeinschaft, DFG) in the framework of the Research Unit FOR2824. SS and DM acknowledge the computational resources provided by the HPC Core Facility and the HRZ of the Justus-Liebig-Universität Gießen. Calculations for this research were also conducted on the Lichtenberg high performance computer of the TU Darmstadt, and at Höchstleistungrechenzentrum Stuttgart (HLRS). We thank Dr. Jonathan Becker and Prof. Müller-Buschbaum for the single crystal XRD measurements.

References

(1) Lloyd, M. A.; Brock, C. P. Retention of $\overline{4}$ Symmetry in Compounds Containing $M\mathrm{Ar}\overline{4}$ Molecules and Ions. *Acta Crystallographica Section B* **1997**, *53*, 780–786.

(2) Hollemann, A. F.; Wiberg, E. *Lehrbuch der Anorganischen Chemie*, 102nd ed.;

Walter de Gruyter, 2007; Stark umgearbeitete und verbesserte Auflage von Nils Wiberg.

(3) Robinson, M. R.; Wang, S.; Heeger, A. J.; Bazan, G. C. A Tetrahedral Oligo(phenylenevinylene) Molecule of Intermediate Dimensions: Effect of Molecular Shape on the Morphology and Electroluminescence of Organic Glasses. *Advanced Functional Materials* **2001**, *11*, 413–419.

(4) Chan, L.-H.; Lee, R.-H.; Hsieh, C.-F.; Yeh, H.-C.; Chen, C.-T. Optimization of High-Performance Blue Organic Light-Emitting Diodes Containing Tetraphenylsilane Molecular Glass Materials. *Journal of the American Chemical Society* **2002**, *124*, 6469–6479.

(5) Yeh, H.-C.; Lee, R.-H.; Chan, L.-H.; Lin, T.-Y. J.; Chen, C.-T.; Balasubramaniam, E.; Tao, Y.-T. Synthesis, Properties, and Applications of Tetraphenylmethane-Based Molecular Materials for Light-Emitting Devices. *Chemistry of Materials* **2001**, *13*, 2788–2796.

(6) Zhou, X.; Huang, M.; Zeng, X.; Chen, T.; Xie, G.; Yin, X.; Yang, C. Combining the qualities of carbazole and tetraphenyl silane in a desirable main chain for thermally activated delayed fluorescence polymers. *Polym. Chem.* **2019**, *10*, 4201–4208.

(7) Sumsion, H. T.; McLachlan, D. The structure of tetraphenylmethane. *Acta Crystallographica* **1950**, *3*, 217–219.

(8) Gruhnert, V.; Kirfel, A.; Will, G.; Wallrafen, F.; Recker, K. The crystal structure and electron density of tetraphenyl-silicon, $(C_6H_5)_4Si$. *Zeitschrift für Kristallographie - Crystalline Materials* **1983**, *163*, 53–60.

(9) Karipides, A.; Haller, D. A. The crystal structure of tetraphenylgermanium. *Acta Crystallographica Section B* **1972**, *28*, 2889–2892.

(10) Belsky, V.; Simonenko, A.; Reikhsfeld, V.; Saratov, I. Structures of tetraphenyltin (redetermination) and tetra(o-tolyl)tin. *Journal of Organometallic Chemistry* **1983**, *244*, 125–128.

(11) Preut, H.; Huber, F. Redetermination of tetraphenyllead. *Acta Crystallographica Section C* **1993**, *49*, 1372–1373.

(12) Smith, A. Low frequency vibrational spectra of group IV-A phenyl compounds. *Spectrochim. Acta, Part A* **1968**, *24*, 695–706.

(13) Smith, A. Vibrational spectra and assignments for the phenyl chlorosilanes. *Spectrochim. Acta, Part A* **1967**, *23*, 1075–1087.

(14) Kriegsmann, H.; Geissler, H. Untersuchungen an Zinnverbindungen. VI. Infrarot- und ramanspektroskopische Untersuchungen an Phenylzinnverbindungen. *Z. Anorg. Allg. Chem.* **1963**, *323*, 170–189.

(15) Durig, J.; Sink, C.; Turner, J. The vibrational spectra and structure of organogermanes - VI Low wavenumber vibrations of (C_6H_54Ge) and $(C_6D_5)_4Ge$. *Spectrochim. Acta, Part A* **1970**, *26*, 557–567.

(16) Clark, R. J. H.; Davies, A. G.; Puddephatt, R. J. Vibrational spectra and structure of organolead compounds. II. Tetraphenyllead, hexaphenyldilead, triphenyllead halides, and diphenyllead dihalides. *Inorg. Chem.* **1969**, *8*, 457–463.

(17) Zelei, B. Vibrational spectra and infrared dichroism of tetraphenylmethane, Ph_4C. *Spectrochim. Acta, Part A* **1986**, *42*, 1119–1125.

(18) Varsányi, G.; Zelei, B.; Dobos, S.; Gál, M. Vibrational spectra and i.r. dichroism of tetraphenyl-silane, Ph_4Si. I. *Spectrochim. Acta, Part A* **1984**, *40*, 529–538.

(19) Schlotter, N. E.; Hudson, B. Tetraphenyl-group IV B compounds: Flexible

molecules with high symmetry crystals. I. Assignment of low frequency infrared and Raman bands. *J. Chem. Phys.* **1982**, *76*, 4844–4856.

(20) Varsányi, G.; Zelei, B.; Kósa, K.; Gál, M. Vibrational spectra and infrared dichroism of tetraphenyl-silane, Ph_4Si. II. *J. Mol. Struct.* **1984**, *115*, 189–192.

(21) Fournier, J.-H.; Wang, X.; Wuest, J. D. Derivatives of tetraphenylmethane and tetraphenylsilane: Synthesis of new tetrahedral building blocks for molecular construction. *Canadian Journal of Chemistry* **2003**, *81*, 376–380.

(22) Busetti, V.; Mammi, M.; Signor, A.; Del Pra, A. A refinement of the crystal structure of tetraphenyl-lead. *Inorganica Chimica Acta* **1967**, *1*, 424–428.

(23) Glidewell, C.; Sheldrick, G. M. Crystal and molecular structure of tetraphenylsilane. *J. Chem. Soc. A* **1971**, 3127–3129.

(24) Sengupta, S.; Sadhukhan, S. K.; Muhuri, S. A tetraphenylmethane based starburst triarylamine cluster: spectroscopy, electrochemistry and morphological studies. *Tetrahedron Letters* **2002**, *43*, 3521–3524.

(25) Campanelli, A. R.; Ramondo, F.; Domenicano, A.; Hargittai, I. Stereoelectronic Effects in the Si-C Bond:âĂĽA Study of the Molecular Structure and Conformation of Tetraphenylsilane by Gas-Phase Electron Diffraction and Theoretical Calculations. *The Journal of Physical Chemistry A* **2001**, *105*, 5933–5939.

(26) Knop, O.; Rankin, K. N.; Cameron, T. S.; Boyd, R. J. Crystal chemistry of tetraradial species. Part 10. Tilting at windmills: conformations of the tetraphenyl species ZPh_4, (Z = B, C, N). *Canadian Journal of Chemistry* **2002**, *80*, 1351–1366.

(27) Tingting, L.; Xue-Ming, L.; Chaobin, H. Ab initio investigation of the structural and electronic properties of the molecules and crystals of tetraphenyl derivatives of group IVA elements. *Journal of Physical Chemistry B* **2004**, *108*, 17361–17368.

(28) Claborn, K.; Kahr, B.; Kaminsky, W. Calculations of optical properties of the tetraphenyl-X family of isomorphous crystals (X = C, Si, Ge, Sn, Pb). *CrystEngComm* **2002**, *4*, 252–256.

(29) Dehnen, S.; Schreiner, P. R.; Chatterjee, S.; Volz, K.; Rosemann, N. W.; Pilgrim, W.-C.; Mollenhauer, D.; Sanna, S. Amorphous Molecular Materials for Directed Supercontinuum Generation. *ChemPhotoChem n/a*.

(30) Rosemann, N. W.; Eußner, J. P.; Beyer, A.; Koch, S. W.; Volz, K.; Dehnen, S.; Chatterjee, S. A highly efficient directional molecular white-light emitter driven by a continuous-wave laser diode. *Science* **2016**, *352*, 1301–1304.

(31) Rosemann, N. W.; Eußner, J. P.; Dornsiepen, E.; Chatterjee, S.; Dehnen, S. Organotetrel Chalcogenide Clusters: Between Strong Second-Harmonic and White-Light Continuum Generation. *Journal of the American Chemical Society* **2016**, *138*, 16224–16227.

(32) Dornsiepen, E.; Dobener, F.; Mengel, N.; Lenchuk, O.; Dues, C.; Sanna, S.; Mollenhauer, D.; Chatterjee, S.; Dehnen, S. White-Light Generation Upon In-Situ Amorphization of Single Crystals of $[(Me_3P)_3AuSn(PhSn)_3S_6]$ and $[(Et_3P)_3AgSn(PhSn)_3S_6]$. *Advanced Optical Materials* **2019**, *7*.

(33) Hanau, K.; Schwan, S.; Schäfer, M. R.; Müller, M. J.; Dues, C.; Rinn, N.; Sanna, S.; Chatterjee, S.; Mollenhauer, D.; Dehnen, S. Towards Understanding the Reactivity and Optical Properties of Organosilicon Sulfide Clusters. *Angewandte Chemie - International Edition* **2021**, *60*, 1176–1186.

(34) Kresse, G.; Furthmüller, J. Efficiency of ab-initio total energy calculations for metals and semiconductors using a plane-wave basis set. *Computational Materials Science* **1996**, *6*, 15 – 50.

(35) Kresse, G.; Furthmüller, J. Efficient iterative schemes for ab initio total-energy calculations using a plane-wave basis set. *Phys. Rev. B* **1996**, *54*, 11169–11186.

(36) Kresse, G.; Joubert, D. From ultrasoft pseudopotentials to the projector augmented-wave method. *Phys. Rev. B* **1999**, *59*, 1758–1775.

(37) Blöchl, P. E. Projector augmented-wave method. *Phys. Rev. B* **1994**, *50*, 17953–17979.

(38) Perdew, J. P.; Chevary, J. A.; Vosko, S. H.; Jackson, K. A.; Pederson, M. R.; Singh, D. J.; Fiolhais, C. Atoms, molecules, solids, and surfaces: Applications of the generalized gradient approximation for exchange and correlation. *Phys. Rev. B* **1992**, *46*, 6671–6687.

(39) Perdew, J. P.; Burke, K.; Ernzerhof, M. Generalized Gradient Approximation Made Simple. *Phys. Rev. Lett.* **1996**, *77*, 3865–3868.

(40) Perdew, J. P.; Burke, K.; Ernzerhof, M. Generalized Gradient Approximation Made Simple [Phys. Rev. Lett. 77, 3865 (1996)]. *Phys. Rev. Lett.* **1997**, *78*, 1396–1396.

(41) Feynman, R. P. Forces in Molecules. *Phys. Rev.* **1939**, *56*, 340–343.

(42) Grimme, S.; Antony, J.; Ehrlich, S.; Krieg, H. A consistent and accurate ab initio parametrization of density functional dispersion correction (DFT-D) for the 94 elements H-Pu. *The Journal of Chemical Physics* **2010**, *132*, 154104.

(43) Grimme, S. Semiempirical GGA-type density functional constructed with a long-range dispersion correction. *Journal of Computational Chemistry* **2006**, *27*, 1787–1799.

(44) Monkhorst, H. J.; Pack, J. D. Special points for Brillouin-zone integrations. *Phys. Rev. B* **1976**, *13*, 5188–5192.

(45) Weyrich, K. H. "Frozen" phonon calculations: Lattice dynamics and -Instabilities. *Ferroelectrics* **1990**, *104*, 183–194.

(46) Weissker, H.-C.; Furthmüller, J.; Bechstedt, F. Structure- and spin-dependent excitation energies and lifetimes of Si and Ge nanocrystals from ab initio calculations. *Phys. Rev. B* **2004**, *69*, 115310.

(47) Riefer, A.; Rauls, E.; Schmidt, W. G.; Eberhard, J.; Stoll, I.; Mattay, J. 2-Aminopyrimidine-silver(I) based organic semiconductors: Electronic structure and optical response. *Phys. Rev. B* **2012**, *85*, 165202.

(48) Heyd, J.; Scuseria, G. E.; Ernzerhof, M. Hybrid functionals based on a screened Coulomb potential. *The Journal of Chemical Physics* **2003**, *118*, 8207–8215.

(49) Hedin, L. New Method for Calculating the One-Particle Green's Function with Application to the Electron-Gas Problem. **1965**, *139*, 796–823.

(50) Krukau, A. V.; Vydrov, O. A.; Izmaylov, A. F.; Scuseria, G. E. Influence of the exchange screening parameter on the performance of screened hybrid functionals. *The Journal of Chemical Physics* **2006**, *125*, 224106.

(51) Gajdoš, M.; Hummer, K.; Kresse, G.; Furthmüller, J.; Bechstedt, F. Linear optical properties in the projector-augmented wave methodology. *Phys. Rev. B* **2006**, *73*, 045112.

(52) Leitsmann, R.; Schmidt, W. G.; Hahn, P. H.; Bechstedt, F. Second-harmonic polarizability including electron-hole attraction from band-structure theory. *Phys. Rev. B* **2005**, *71*, 195209.

(53) Riefer, A.; Sanna, S.; Schindlmayr, A.; Schmidt, W. G. Optical response of stoichiometric and congruent lithium niobate from first-principles calculations. *Phys. Rev. B* **2013**, *87*, 195208.

(54) Attaccalite, C.; Grüning, M.; Marini, A. Real-time approach to the optical properties of solids and nanostructures: Time-dependent Bethe-Salpeter equation. *Phys. Rev. B* **2011**, *84*, 245110.

(55) Attaccalite, C.; Grüning, M. Nonlinear optics from an ab initio approach by means of the dynamical Berry phase: Application to second- and third-harmonic generation in semiconductors. *Phys. Rev. B* **2013**, *88*, 235113.

(56) Souza, I.; Íñiguez, J.; Vanderbilt, D. Dynamics of Berry-phase polarization in time-dependent electric fields. *Phys. Rev. B* **2004**, *69*, 085106.

(57) `http://www.turbomole.com`, TURBOMOLE v7.3 2018. A development of University of Karlsruhe and Forschungeszentrum Karlsruhe GmbH, 1989-2007, TURBOMOLE GmbH.

(58) Eichkorn, K.; Treutler, O.; Öhm, H.; Häser, M.; Ahlrichs, R. Auxiliary basis sets to approximate Coulomb potentials. *Chemical Physics Letters* **1995**, *240*, 283–290.

(59) Slater, J. C. A Simplification of the Hartree-Fock Method. *Phys. Rev.* **1951**, *81*, 385–390.

(60) Perdew, J. P.; Wang, Y. Accurate and simple analytic representation of the electron-gas correlation energy. *Phys. Rev. B* **1992**, *45*, 13244–13249.

(61) Grimme, S.; Ehrlich, S.; Goerigk, L. Effect of the damping function in dispersion corrected density functional theory. *Journal of Computational Chemistry* **2011**, *32*, 1456–1465.

(62) Dunning, T. H. Gaussian basis sets for use in correlated molecular calculations. I. The atoms boron through neon and hydrogen. *The Journal of Chemical Physics* **1989**, *90*, 1007–1023.

(63) Kendall, R. A.; Dunning, T. H.; Harrison, R. J. Electron affinities of the first-row atoms revisited. Systematic basis sets and wave functions. *The Journal of Chemical Physics* **1992**, *96*, 6796–6806.

(64) Peterson, K. A. Systematically convergent basis sets with relativistic pseudopotentials. I. Correlation consistent basis sets for the post-d group 13-15 elements. *The Journal of Chemical Physics* **2003**, *119*, 11099–11112.

(65) Metz, B.; Stoll, H.; Dolg, M. Small-core multiconfiguration-Dirac-Hartree-Fock adjusted pseudopotentials for post-d main group elements: Application to PbH and PbO. *The Journal of Chemical Physics* **2000**, *113*, 2563–2569.

(66) Runge, E.; Gross, E. K. U. Density-Functional Theory for Time-Dependent Systems. *Phys. Rev. Lett.* **1984**, *52*, 997–1000.

(67) Gross, E. K. U.; Kohn, W. In *Density Functional Theory of Many-Fermion Systems*; Löwdin, P.-O., Ed.; Advances in Quantum Chemistry; Academic Press, 1990; Vol. 21; pp 255–291.

(68) Bauernschmitt, R.; Ahlrichs, R. Stability analysis for solutions of the closed shell Kohn-Sham equation. *The Journal of Chemical Physics* **1996**, *104*, 9047–9052.

(69) Bauernschmitt, R.; Ahlrichs, R. Treatment of electronic excitations within the adiabatic approximation of time dependent density functional theory. *Chemical Physics Letters* **1996**, *256*, 454–464.

(70) Perdew, J. P.; Ernzerhof, M.; Burke, K. Rationale for mixing exact exchange with density functional approximations. *The*

Journal of Chemical Physics **1996**, *105*, 9982–9985.

(71) Newkirk, H. W. Piezoelectric organometallic crystal: Growth and properties of tetraphenylsilicon, -germanium, -ti and -lead. *Journal of Organometallic Chemistry* **1972**, *44*, 263–271.

(72) Levine, B.; Bethea, C. Nonlinear susceptibility of GaP; relative measurement and use of measured values to determine a better absolute value. *Applied Physics Letters* **1972**, *20*, 272–275.

(73) Miller, R. C. Optical second harmonic generation in piezoelectric crystals. *Applied Physics Letters* **1964**, *5*, 17–19.

(74) Schmidt, F.; Riefer, A.; Schmidt, W. G.; Schindlmayr, A.; Imlau, M.; Dobener, F.; Mengel, N.; Chatterjee, S.; Sanna, S. Quasiparticle and excitonic effects in the optical response of $KNbO_3$. *Phys. Rev. Materials* **2019**, *3*, 054401.

(75) Berreman, D. W. Optics in Stratified and Anisotropic Media: 4×4-Matrix Formulation. *J. Opt. Soc. Am.* **1972**, *62*, 502–510.

(76) Müller, M. J.; Dobener, F. pyElli. 2021; `https://doi.org/10.5281/zenodo.5702470`.

(77) Csákvári, É.; Shishkov, I. F.; Rozsondai, B.; Hargittai, I. Determination of the gas-phase molecular structures of tetraphenylsilane, tetraphenylgermane, and tetraphenyltin by electron diffraction. *Journal of Molecular Structure* **1990**, *239*, 291–303.

(78) Ismailzade, I. G.; Zhdanov, G. S. *Zhur. Fiz. Khim.* **1952**, *26*, 1619.

(79) Höfler, F. Modellberechnugnen zu den Schwingungsspektren von Phenylsilanen und einigen verwandten Verbindungen. *Monatsh. Chem.* **1976**, *107*, 705–719.

(80) La Paglia, S. Singlet-triplet transitions in the tetraphenyls. *Spectrochimica Acta* **1962**, *18*, 1295–1298.

(81) Boyd, R. W. In *Nonlinear Optics (Third Edition)*, third edition ed.; Boyd, R. W., Ed.; Academic Press: Burlington, 2008; pp 1–67.

(82) Butcher, P. *Nonlinear Optical Phenomena*; Bulletin (Ohio State University. Engineering Experiment Station : 1963); Engineering Experiment Station, Ohio State University, 1965.

Graphical TOC Entry

Some journals require a graphical entry for the Table of Contents. This should be laid out "print ready" so that the sizing of the text is correct.
Inside the `tocentry` environment, the font used is Helvetica 8 pt, as required by *Journal of the American Chemical Society*.
The surrounding frame is 9 cm by 3.5 cm, which is the maximum permitted for *Journal of the American Chemical Society* graphical table of content entries. The box will not resize if the content is too big: instead it will overflow the edge of the box.
This box and the associated title will always be printed on a separate page at the end of the document.